

Chapter 2

The Chest Wall and the Respiratory Pump

Abstract The design of the respiratory pump is different from the design of the heart. The ribs carry compressive stresses that balance the pressure difference across the chest wall, and the rib cage provides a mechanism for transforming muscle shortening into chest wall expansion. The external intercostal muscles in the cranial-dorsal quadrant and the parasternal muscles have inspiratory actions and the internal intercostals in the caudal-dorsal quadrant and the triangularis sterni have expiratory actions. The diaphragm separates the pleural cavity and the abdomen, and the combined effect of diaphragm muscle tension and curvature balances the difference between abdominal pressure and pleural pressure. The inspiratory action of the diaphragm is the result of the descent of the diaphragm that accompanies muscle shortening and of the inspiratory forces that the diaphragm exerts on the lower ribs. Compartmental models provide simplified descriptions of the mechanics of the chest wall. The work of breathing is small compared to the work of the heart.

2.1 Design of the Respiratory Pump

Respiratory gasses are transported between the ambient air and the tissues of the body by a two-fluid system: gaseous transport between the atmosphere and the lungs, and transport via blood between the lungs and the tissues. Pumps are needed to drive the flows of both fluids. The heart beats five times as fast as the respiratory pump, but the stroke volume of the respiratory pump is five times that of the heart, and because the oxygen carrying capacity of air and blood per unit volume are about the same, the rates of fluid displacement for the two pumps are about the same. However, the driving pressure developed by the heart is 20 times that developed by the respiratory pump, and hence the work done is 20 times greater. This difference is ultimately due to the higher viscosity of water than air (by a factor of 25) and the much lower diffusivities of metabolic gases in water than in air (by a factor of 10^4). In fish, the relationship between the two pumps is quite different.

Although the respiratory pump is as essential as the circulatory pump, the respiratory pump has received little attention compared to the attention given to the heart. Why is that? Perhaps because the muscles of the respiratory pump are

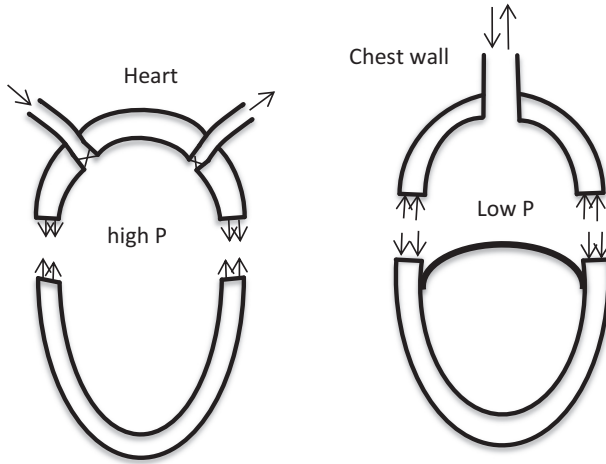


Fig. 2.1 Comparison between the designs of the circulatory and respiratory pumps

dispersed and multi-functional whereas the heart provides a clear focus. Probably, the more important reason is that the respiratory pump rarely fails, except through failure of innervation due to accidental nerve damage or degenerative nerve or muscle disease, whereas heart failure is a prominent medical problem.

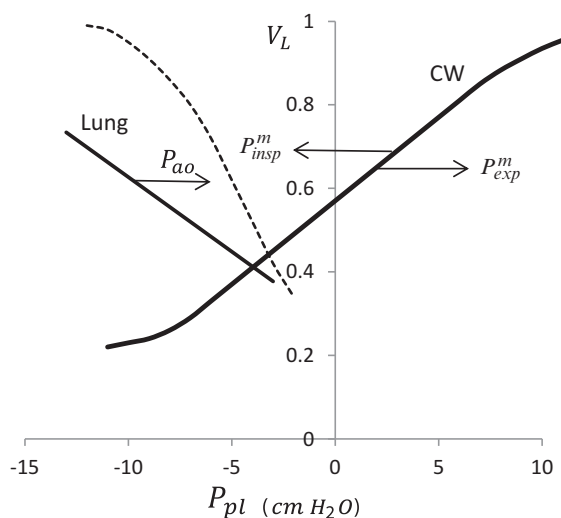
The two pumps have different designs. These designs are illustrated in Fig. 2.1. The heart is a flow-through system with valves. In the heart, pressure is increased in the fluid in the chamber, and flow is driven by contraction of the volume of the chamber. Tension is required in the wall of the heart to balance the pressure in the chamber, and work is done as the heart contracts. Both of these requirements on heart wall mechanics match the capabilities of muscle; muscle develops tension when it is activated, and muscles do work when they contract. Therefore, the wall of the heart can be made of muscle.

In contrast, the respiratory pump is a batch-processing system with the same path for inflow and outflow. In the respiratory pump, pressure is reduced in the thoracic cavity to draw air into the lungs, and flow is driven by expansion of the chest wall. The wall of the chamber must therefore carry compressive stress, and the wall must expand as it does work. These requirements are contrary to the capability of muscles. This problem is solved in two ways. First, part of the chamber wall is inverted so that it is concave outward. In this part, tension in the wall balances the low pressure inside the chamber and chamber volume expands as the wall contracts. Thus, this part, the diaphragm, can be made of muscle and tendon. However, part of the wall must be concave inward. If this part is to participate in the pumping action, bones are required to carry the compressive stress, and a mechanism is required to convert muscle contraction into volume expansion [1]. The ribs and sternum fulfill these requirements.

The chest wall consists of the structures that bound the lungs and participate in breathing: the rib cage, heart, diaphragm, and abdomen. To be compatible with the variables that are used to describe the mechanics of the lung, pressure and volume are used to describe the mechanics of the chest wall. The passive chest wall and the pleural cavity expand as pleural pressure on the inner surface of the chest wall is increased. The pressure—volume curve for the passive chest wall (CW) is shown in Fig. 2.2 along with pressure-volume curves for the lung. In this figure, lung volume (V_L), expressed as a fraction of total lung capacity (TLC), is plotted against pleural pressure (P_{pl}). The lung and chest wall must have the same volume and be exposed to the same value of P_{pl} , and the equilibrium state for the system is given by the intersection between the $P_{pl} - V_L$ curves for the lung and chest wall. Pleural pressure at this equilibrium point is approximately -4 cm H₂O, and lung volume, denoted functional residual capacity (FRC), is about 40 % TLC.

During passive inflation of the respiratory system, pressure at the airway opening (P_{ao}) is increased. This shifts the pressure volume curve of the lung to the right and raises the equilibrium values of P_{pl} and V_L . During active breathing, the chest wall is expanded or compressed by action of the respiratory muscles. To describe the action of the muscles in Fig. 2.2, their action must be described as effective inspiratory or expiratory pressures exerted by the muscles, denoted P_{insp}^m or P_{exp}^m . P_{insp}^m shifts the curve for the chest wall to the left, raises V_L , and lowers P_{pl} . P_{exp}^m shifts the curve to the right. Much of the study of the respiratory pump focuses on evaluating the effective pressures exerted by the respiratory muscles.

Fig. 2.2 Lung volume (V_L) as a fraction of TLC vs. pleural pressure (P_{pl}) for the passive chest wall (CW) and the lung for tidal volume oscillations (*solid line*) and deflation from TLC (*dashed line*)



2.2 Rib Cage and Intercostal Muscles

The head of each rib inserts into facets on the edges of two adjacent vertebrae. The neck of the rib extends from the head to a connection between matching facets on the rib and on the transverse process of the lower vertebra and then on to the posterior angle of the rib. Thus, the seat at the head of the rib and the connection to the transverse process define an axis around which the rib rotates. However, the facets at the transverse process are shallow and may allow some translational as well as rotational displacements. The shaft of the rib forms a smooth arc that extends from the posterior angle to the connection to the lateral end of the costal cartilage. The arc of the shaft lies nicely in a plane over most of its length with some torsion near the ventral end. In dogs, the widths of the ribs and interspaces are ~ 0.4 and 1.3 cm; in humans, 1.2 and 2.3 cm. The costal cartilage links the ends of the ribs to the sternum. In dogs, the costal cartilage slants sharply caudally from the sternum to the rib. In humans, it is nearly horizontal for the upper ribs and angles downward with increasing rib number. In humans, the cartilage connections for ribs 7–10 do not extend to the sternum; they connect to the cartilage of the rib above, and the ends of ribs 11 and 12 are unconnected.

The system for describing the geometry of the ribs is shown in Fig. 2.3, and the values of the parameters for the rib cage of 12 kg dog [2] and human ribs [3] are given in the Appendix. Center lines of the ribs at FRC and TLC are shown in Fig. 2.4, and the values of α and β at FRC and the rotations $\delta\alpha$ and $\delta\beta$ from FRC to TLC are shown in Fig. 2.5. These are denoted the “pump handle” and “bucket handle” rotations, respectively.

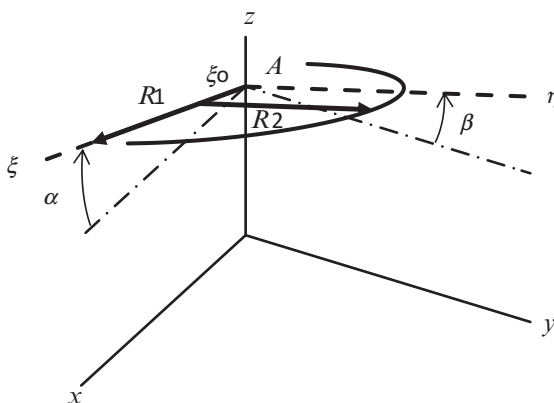


Fig. 2.3 Parameters used to describe the geometry of the ribs on the left side of the rib cage. The x axis runs ventrally and the y axis laterally. The ribs lie in the ξ – η plane which intersects the z axis at A . The ξ axis is inclined to the x axis by angle α and the η axis is inclined to the y axis by angle β . In dogs, β is negative and in humans α is negative. The line of the rib in the plane is given by $\xi = \xi_0 + R_1 \cdot \sin\theta$, $\eta = R_2 \cdot \cos\theta$

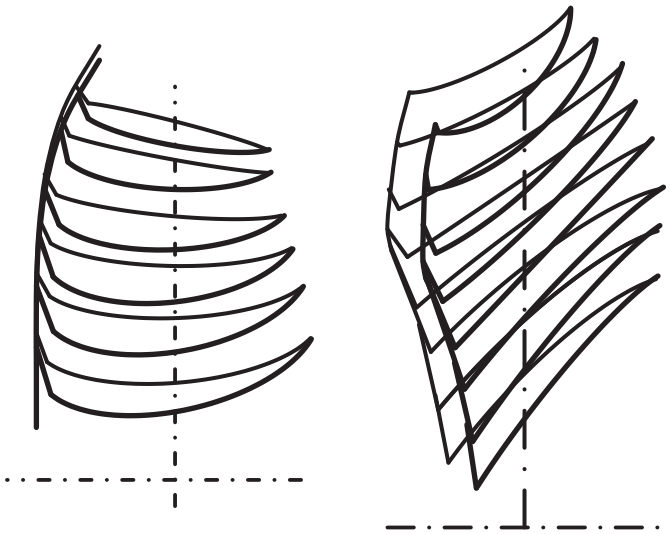


Fig. 2.4 Lateral view of the center lines of ribs 3–8 of the dog (*left panel*) and ribs 2–9 of human (*right panel*) at FRC (*heavier lines*) and TLC (*lighter lines*)

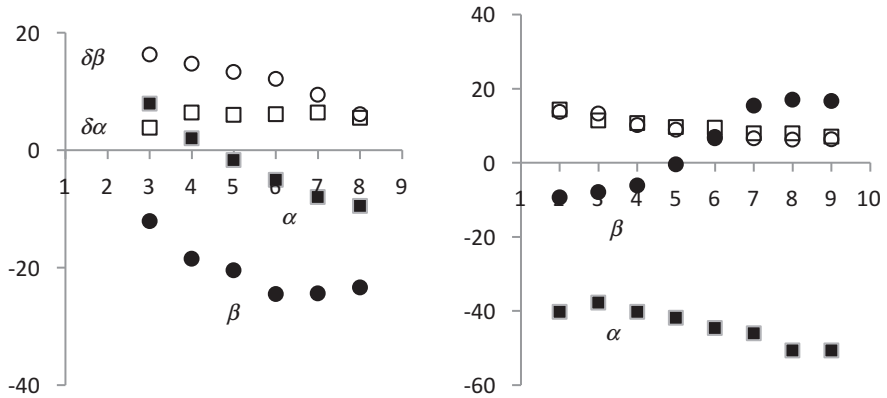


Fig. 2.5 Values of α (*filled squares*) and β (*filled circles*) at FRC and changes in the angles (*open symbols*) for rib rotations from FRC to TLC vs. rib number in the dog (*left panel*) and human (*right panel*)

It can be seen from these figures that in the dog, the ribs slant laterally and in humans, ventrally. In the dog, $\delta\beta$ is larger than $\delta\alpha$, and in humans, they are about equal. The magnitudes of total rib rotation are about the same in both species, decreasing from $\sim 17^\circ$ for the third rib to $\sim 10^\circ$ for the eighth.

The only component of rib displacement that acts to increase the volume of the thorax is the component normal to the surface. In dogs, the lateral surface area is bigger than the ventral area, the lateral slant is greater, and the lateral displacements

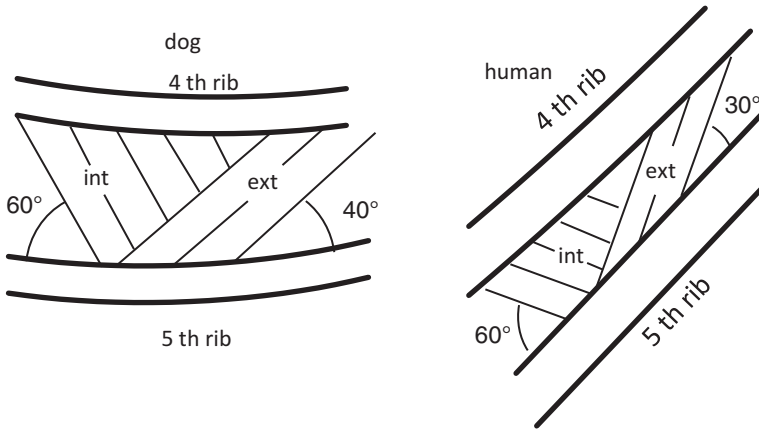


Fig. 2.6 Intercostal muscle orientation in the fourth interspace

are larger than the ventral displacements. As a result, the rib cage expands primarily through expansion in the lateral direction. In humans, the ventral surface is larger than the lateral surface, the ventral slant is larger, and the thorax expands primarily in the dorso-ventral direction. Because the rib cage tapers inward cranially, cranial displacements also contribute to expansion of the thorax, but the cranial displacement is less effective [4].

In human infants, the angle α is small, as it is in dogs. The caudal slant develops at about age two when children begin to walk. This fact is provocative, but in thinking about design, it should be kept in mind that ribs have other functions in addition to their respiratory function. A visit to the natural history museum illustrates this point; the ribs of many dinosaurs continue past the shoulders and out along the neck.

Intercostal muscles lie in two layers, the internal and external intercostals. The internal intercostals extend from the sternum to near the spine, and the externals extend from the condro-costal junction to the angle of the rib and carry on to the spine with the levator costae. The exposed portion of the internal intercostals near the sternum are termed the parasternals. The geometry of ribs and muscle on the lateral surface of the fourth interspace in the two species are shown in Fig 2.6. In both species the lines of the muscle bundles of the two layers are nearly orthogonal.

2.2.1 *Respiratory Effect of the Muscles*

The respiratory action of the intercostals has been a conundrum. Galen thought that both layers have an expiratory effect. Leonardo argued that the externals would raise the ribs and have an inspiratory effect, and that the internals would have an expiratory effect. Subsequently, the remaining two possible functional

combinations were proposed. It has not been possible to activate individual segments of the individual layers of the intercostal muscles to experimentally determine their respiratory effect.

Recently, these questions have been resolved, and new data have been obtained that improve our understanding of intercostal action. A theorem of mechanics that governs linear elastic systems, applied to the respiratory system, yields the following equations [5].

$$\Delta Pao = m \cdot \sigma \cdot \mu \quad \mu = [dl/l \cdot dVL]_{rel} \quad (2.1)$$

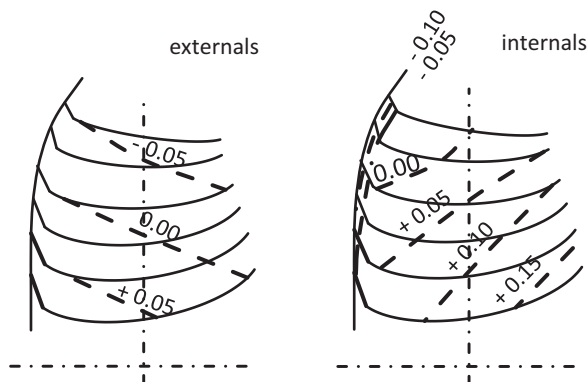
The first of these equations is simply a definition of the mechanical advantage of a muscle, denoted μ . Thus, μ is defined as the change in Pao per unit active stress σ and per unit muscle mass m when the muscle is activated with the airway occluded. The second equation provides the method for evaluating μ . This equation states that μ equals the fractional change in muscle length, dl/l , per unit change in lung volume, dV_L , during passive inflation of the lungs (*rel*). For muscle mass expressed in g, σ in kg/cm^2 , and μ in L^{-1} , Eq. (2.1) yields ΔPao in $\text{cm H}_2\text{O}$.

Equation (2.1) provides a method for assessing the respiratory effect of the respiratory muscles. Qualitatively, muscles that shorten during passive inflation have negative values of μ and have an inspiratory effect, and muscles that lengthen have an expiratory effect. The quantitative maximum potential respiratory effect is obtained by measuring muscle mass and fractional change in length per unit volume increase during passive inflation and multiplying the product $m \cdot \mu$ by the maximum active stress in skeletal muscles, $3.0 \text{ kg}/\text{cm}^2$. For muscles that can be individually activated in the dog, namely, the parasternals in different interspaces, the scalenes, sternomastoids, and triangularis sterni, the measured ΔPao agrees extremely well with that predicted from Eq. (2.1) [6].

The rib displacements described above produce shear strains in the interspaces and compression of the upper interspaces and dilatation of the lower interspaces. The fractional length change of a muscle depends on interspace number, position around the circumference of the rib, and muscle orientation. μ was evaluated in dogs by inserting screws at the ends of muscle bundles and directly measuring the distance between the screws at FRC and after increasing lung volume to TLC [7, 8]. In humans, μ was evaluated by calculating muscle lengths from the data on rib geometry at FRC and TLC [3, 9]. The results for dogs are more certain and more detailed and the level lines for the distribution of μ for the intercostal muscles of dogs are shown in Fig. 2.7. The values in Fig. 2.7 are average values over the range of lung volumes from FRC to TLC.

The external intercostals have a potential inspiratory effect in the cranial-dorsal region of the rib cage and a potential expiratory effect in the caudal-ventral region. The internals have a potential expiratory effect in the caudal-dorsal region, and the parasternals have a strong potential inspiratory effect. Thus, both the externals and internals have potential effects of both signs, and their functional action depends on the distribution of muscle activation during inspiration and expiration.

Fig. 2.7 Level lines for the distribution of mechanical advantage (μ) of the external and internal intercostal muscles of the dog. The data described here are for 24 kg dogs



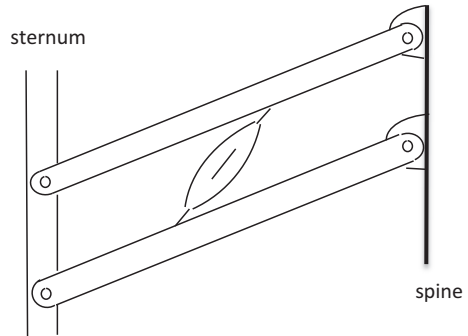
Only the external intercostals with inspiratory effect and the parasternals are activated during inspiration and only the internal intercostals with expiratory effect are activated during active expiration. Moreover, the distribution of activation mirrors the magnitude of mechanical advantage [10–12]. In the external intercostals, the level of inspiratory activation is greatest in the cranial-dorsal corner, and in the parasternals, in the upper interspaces and closest to the sternum. With increasing inspiratory effort, the level of activation in those regions increases and activation spreads to regions with a smaller magnitude of inspiratory mechanical advantage. Furthermore, the distribution of muscle mass mimics the distribution of mechanical advantage. The thickness of the externals is greatest in the cranial-dorsal corner and decreases ventrally and caudally. The thickness of the parasternals is greater than that of the external intercostals and decreases laterally and caudally. The calculated maximum total inspiratory effect of the intercostals is $-18 \text{ cm H}_2\text{O}$. This agrees with the observation of DiMarco et al. [13, 14] for the value of ΔP_{ao} during maximal activation of the inspiratory intercostals. This maximum effect decreases with increasing lung volume.

The distribution of mechanical advantage of the human intercostals is like that of the dog. However, whereas the parasternals have a stronger potential effect than the externals in the dog, the opposite is true for humans. The magnitudes of the mechanical advantages of humans are lower than those of the dog by a factor of ~ 3 , and the masses are larger by the same factor; the maximum total effect is about the same.

2.2.2 Mechanisms of Intercostal Muscle Action

Hamberger's theory of intercostal muscle action was presented in his book, published in 1734 [15]. The heart of the book lies in diagrams like that shown in Fig. 2.8. The spine is represented by the vertical bar on the right and two ribs by bars

Fig. 2.8 Hamberger model
for the mechanics of
intercostal muscle action



connected to the spine by pin joints and slanting down to connections to the sternum. An intercostal muscle slants between the two ribs. The normal component of the force exerted on the lower rib exerts a moment around the pin joint on the spine, and the normal component of the equal and opposite force exerted on the upper rib exerts a moment with opposite sign on that rib. Because the moment arm of the force on the lower rib is greater than that on the upper rib, the net moment would cause a cranial rotation of the ribs. This mechanism will be referred to as the Hamberger mechanism. By this analysis, muscles that slant upward to the right of the vertical in Fig. 2.8, as the external intercostals do, would cause a cranial displacement of the ribs and act as inspiratory muscles, and muscles that slant to the left, the internal intercostals, would have an expiratory effect. The conclusion that follows from this model is that all external intercostals have an inspiratory effect and all internal intercostals have an expiratory effect.

Although alternate ideas about intercostal muscle action were expressed throughout the intervening years, the Hamberger model has provided the dominant concept of intercostal mechanics for more than two centuries. The Hamberger model in fact correctly captures one of the mechanisms of intercostal muscle action, but the model has shortcomings. First, the model is two-dimensional whereas the rib cage is three-dimensional. In the diagram, the plane of the ribs is perpendicular to the axis of rib rotation. In the rib cage, the plane of the ribs on the dorsal surface of the rib cage is perpendicular to the axis of rotation, but the angle changes moving ventrally around the rib. On the ventral surface, the plane is parallel to the axis, and the difference in moments on the two ribs is zero. Near the sternum, the net moment changes sign and becomes expiratory. This mechanism explains, in part, the inspiratory effect of the external intercostals and expiratory effect of the internal intercostals on the dorsal surface and the dorsal-ventral gradients in respiratory effect within each interspace.

A second shortcoming of the Hamberger model is that it ignores the coupling between rib displacement and lung expansion. A second mechanism was revealed when the coupling between ribs and lung in dogs was studied by De Troyer et al. [16–18]. Screws were inserted into the ribs on both sides of the rib cage, a yoke was attached to the two screws in the n th rib pair, and airway opening pressure

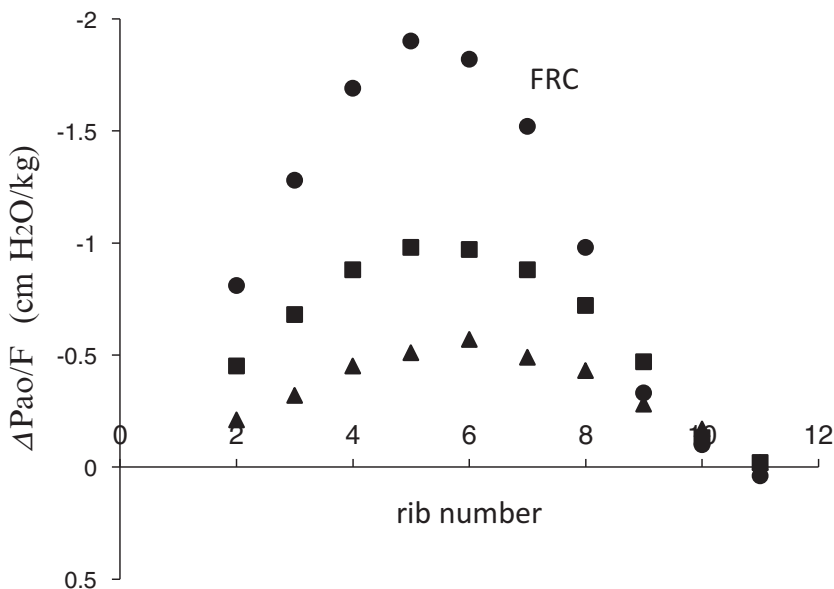


Fig. 2.9 Values of $\Delta P_{ao}/F$ for external forces (F) applied to rib pairs at FRC (*circles*) and higher lung volumes (*squares and triangles*)

was measured as a cranial force was applied to the rib pair with the airway occluded. The results of this experiment are shown in Fig. 2.9. It can be seen that the respiratory effect per unit force varies markedly with rib number. It increases with rib number from the second to fifth rib pair and then decreases to essentially zero for the 11th pair. Rib displacements were also measured, and these were nearly uniform, increasing slightly with increasing rib number. Thus, the strong dependence of ΔP_{ao} on n is not the result of differences in rib compliance. Presumably, it is the result of the dependence of the lung-apposed surface area subtended by the ribs on rib number. For the upper ribs, rib radius and circumference increase with rib number, and thus, the subtended surface area increases with rib number. The lung-apposed area then decreases for the more caudal ribs because the fraction of the subtended area that is apposed to the lung decreases and the fraction that is apposed to the abdomen increases. At higher lung volumes, the dependence of P_{ao}/F on rib number is similar, but the magnitudes decrease markedly with increasing lung volume.

The Hamberger mechanism for muscle action depends on the slant of the intercostals and the resulting difference between the moments exerted on the two ribs that bound the interspace. Figure 2.9 shows that a muscle that is oriented axially would also have a net respiratory effect because the respiratory effects of equal and opposite forces on adjacent ribs are not equal. In the cranial interspaces, the inspiratory effect on the lower rib is greater than the expiratory effect on the upper rib, and the net effect is inspiratory. In the caudal interspaces, the opposite

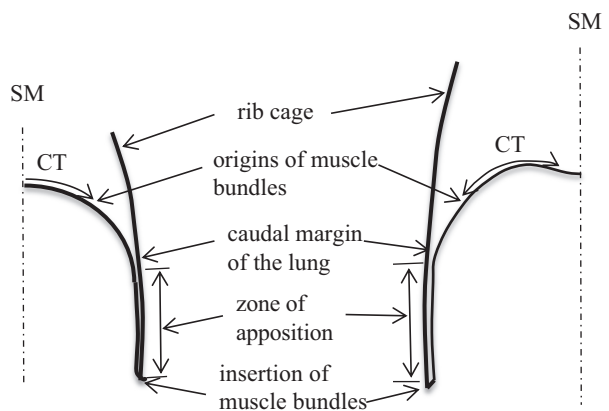
holds. Thus, this mechanism accounts for the cranial-caudal gradient in respiratory effect from generally inspiratory in cranial interspaces to generally expiratory in the caudal interspaces.

2.3 Diaphragm

The diaphragm is a thin membrane that separates the thoracic cavity from the abdomen. It consists of the central tendon, a thin sheet of connective tissue that is functionally inextensible, surrounded by a muscle sheet. The muscle bundles that form this sheet originate at the edge of the central tendon and insert on the upper edge of the lower ribs and on the spine as shown in Fig. 2.10.

In the dog, the central tendon is roughly triangular with the apex at the ventral end and the curved base at the dorsal end. Lines of connective tissue extend from the corners of the base to the spine. The central tendon covers the dome of the diaphragm that is located in the mid-plane. The muscle sheet consists of two parts, the costal diaphragm that extends from the sternum to the most dorsal points on the arcs of the ribs and the crural diaphragm that extends from the dorsal points to the midplane. The muscles bundles of the costal diaphragm insert on the upper edge of the lower ribs, and the bundles of the crural diaphragm insert on the spine. In a number of studies, the length of the diaphragm muscle bundles and the height of the zone of apposition have been underestimated because a band of fatty tissue on the abdominal surface of the diaphragm was identified as the line of insertion. Although the muscles are not visible from the abdominal side below this band, they extend 1–2 cm beyond the fatty band to the true line of insertion [19]. In a 24 kg dog, the length of the muscle bundles is ~4 cm at the ventral end, increasing to ~8 cm on the lateral surface [20]. The central tendon and the muscle sheet near the tendon are apposed to the lung. The distal part of the muscle sheet lies on the inner surface of the rib cage and this region is called the zone of apposition. The line of the top of the zone of apposition (the bottom edge of the lung) lies in a plane that slants downward

Fig. 2.10 Transverse sections through the domes of the diaphragm in the dog (*left*) and human (*right*). The sagittal midplanes (SM) are shown by *interrupted lines* and the central tendons (CT) by *arrows*



from the transverse plane by $\sim 30^\circ$. With increasing lung volume, the muscle shortens, the dome of the diaphragm descends, the rib cage expands and the height of the zone of apposition decreases.

In humans, the central tendon is two-lobed with one lobe covering the dome in each hemi-diaphragm and some fibers of connective tissue connecting the lobes across the saddle point in the mid-plane. The length of the muscle bundles is ~ 6 cm at the ventral end and increases rapidly to ~ 13 cm at the lateral surface. MRI data for humans [21] provide detailed information about the shape of the human diaphragm and the displacements that occur with lung inflation. With inflation from FRC to TLC, the dome descends by ~ 5 cm and the muscles shorten by $\sim 35\%$. The height of the zone of apposition on the lateral surface decreases from ~ 9 cm at FRC to 4.5 cm at TLC. At FRC, seventy percentage of the muscle lies in the zone of apposition, and this decreases to 50 % at TLC.

Mead [22] ascribed four functions to the zone of apposition. First, it provides a reservoir of rib cage surface area so that the base of the lung can descend, relative to the rib cage, without distorting the shape of the lung. Second, expansion of the rib cage in the area apposed to the diaphragm provides a pathway, in addition to the expansion of the abdominal wall, for the volume displaced by the diaphragm. Third, it serves as the site for the application of abdominal pressure to the lower rib cage. Fourth, it serves to direct the force exerted by the diaphragm at the line of insertion in the cranial direction. A fifth function could be added to this list; it provides a reservoir of muscle length so that, for a given descent of the diaphragm, fractional muscle shortening is reduced.

2.3.1 *Respiratory Effect*

The muscles of the diaphragm shorten by 30–35 % with passive lung inflation from FRC to TLC [19, 21, 23]. For a 24 kg dog, therefore, $\mu = -0.25 L^{-1}$. Muscle mass is 95 g [24], and the maximum respiratory effect of the diaphragm is $P_{ao} = -70$ cm H₂O. The proportionality between level of activation and mechanical advantage, described above, applies within each muscle group, but not across groups. In the dog, the mechanical advantage of the diaphragm is twice that of the parasternals, but the level of activation of the diaphragm during spontaneous breathing is always less than maximum [25] whereas the level of activation of the parasternals during vigorous inspiratory efforts approaches 100 %. Thus, it appears that the mass of the diaphragm has been set by other functions.

2.3.2 *Transdiaphragmatic Pressure*

Strains in the two directions in the plane of the muscles of the diaphragm have been measured during spontaneous breathing [26]. Whereas the muscle layer shortens along the line of the muscle bundles, the strain in the direction transverse to the line

of the muscle is essentially zero. The layer is compliant in the transverse direction [27], and it follows that, *in vivo*, the stress in the transverse direction is zero. Thus, the muscle layer is a membrane that carries stress in only one direction, the direction of the muscle fibers. It follows from this that the lines of the muscles must lie along geodesics of the surface. That is, the curvature of the lines is perpendicular to the surface. The lung-apposed diaphragm can be roughly pictured as a slinky laid out around the inner surface of the rib cage with the opening within the ring covered by the central tendon and the tangent line between the slinky and the rib cage forming the upper edge of the zone of apposition [28].

It also follows that the equation of equilibrium for the lung-apposed muscle layer is the following where P_{di} is transdiaphragmatic pressure, t is the thickness of the layer, σ is the stress in the muscle, and ρ is the radius of curvature of the line of the muscle bundle.

$$P_{di} = t \cdot \sigma / \rho \quad (2.2)$$

For the dog, $t = 0.17$ cm [29], $\rho = 4.5$ cm [30], and for maximum stress, 3 kg/cm^2 , $P_{di} = 115 \text{ cm H}_2\text{O}$. This agrees with the value reported by Road et al. [31] for P_{di} for maximum activation of the diaphragm at FRC. The value of ρ remains constant as lung volume increases and muscle length decreases down to 60 % L_o [32], and the measured curve of P_{di} vs. muscle length corresponds to the curve of σ vs. L/L_o for skeletal muscle.

The value of P_{di} , calculated here, is not the same as the value of P_{ao} for the diaphragm calculated earlier. The value of P_{di} , calculated here, is transdiaphragmatic pressure, whereas the value of P_{ao} is the airway pressure that results from activation of the muscle. The relation between the two will be described below.

The inspiratory action of the diaphragm is the result of two mechanisms. First, P_{di} is applied to the boundary between the lung and the abdomen. With increasing P_{di} , the muscles of the diaphragm shorten and the dome of the diaphragm descends, thereby expanding the volume of the thoracic cavity and the lung. With diaphragm descent, pleural pressure falls, abdominal pressure increases, and the abdominal wall expands.

The second mechanism is the result of the two forces exerted by the diaphragm on the rib cage. The first of these, the insertional force, is the axial force exerted by muscle tension acting directly at the line of insertion on the lower margin of the rib cage. This force has been recognized since Galen. The second, the appositional force, was described by Mead in 1979 [22]. This is the lateral pressure that acts on the rib cage in the zone of apposition. In the zone of apposition, the diaphragm is constrained to lie along the surface of the rib cage, and its curvature is less than in the lung-apposed region. The pressure exerted on the rib cage can be described in either of two ways: either as the pressure exerted by the diaphragm on the rib cage because the curvature of the diaphragm is reduced, or alternatively, as the partial or complete transmission of abdominal pressure across the diaphragm because the curvature of the diaphragm is less than that in the lung-opposed region.

Most experimental studies of the action of the diaphragm in dogs have used maximum activation of the phrenic nerves to stimulate diaphragm contraction. This method provides a standard reproducible level of diaphragm activation, but the results are skewed by the fact that maximum diaphragm activation is unphysiological and the distortions of the rib cage that it generates are unphysiological. In 2011, De Troyer introduced a new preparation [33]. He severed the inspiratory intercostal muscles in all interspaces, except the parasternals in one interspace, which were used to monitor neural drive, and he measured the displacements of ribs in the upper and lower rib cage during spontaneous breathing with the diaphragm alone. In this preparation, the rib cage does not move as a unit; at FRC, the upper ribs move caudally and inward and the lower ribs move cranially and outward. This is consistent with the earlier observation that the upper ribs move paradoxically in quadriplegic subjects breathing with their diaphragm alone [34, 35].

The diaphragm is frequently described as a piston that moves caudally as the muscles contract. This analogy is incomplete. The diaphragm is more like a hemiballoon attached to the lower margin of the rib cage and in contact with the chest wall in the zone of apposition. With activation, the dome descends, and the diaphragm pulls cranially and pushes laterally on the lower rib cage, thereby acting as the primary inspiratory muscle for the lower rib cage.

2.3.3 Volume Dependence

The respiratory effect of both the intercostal muscles [13] and the diaphragm [36] decrease markedly with increasing lung volume. The decrease of intercostal effect is primarily due to the change in the geometry of the rib cage [37]; for increased β in the dog or α in man, the component of rib displacement perpendicular to the surface decreases for a given increment in β or α . The decrease in diaphragm effect is due to the decrease in muscle length, and hence muscle force, for a given level of activation.

2.4 Other Respiratory Muscles

In addition to the external intercostals in the cranial interspaces and the parasternals, the pectoralis major and pectoralis minor that lie on the ventral surface of the upper rib cage are activated during inspiration, but only during extreme efforts.

Two of the muscles of the neck act as inspiratory muscles, the scalenes and the sternomastoids. In humans, the scalenes run from the transverse processes of the lower cervical vertebrae to the upper surface of the first two ribs. The sternomastoids

run from the mastoid process to the manubrium sterni and the clavicle. In dogs, both muscles are silent during quiet breathing and are recruited during more forceful inspiration. In humans, the scalenes are active during quiet breathing and the sternomastoids are recruited during more forceful inspiration. These muscles add a potential maximum inspiratory effect of ≈ -6 cm H₂O [38, 39].

In addition to the internal intercostals in the caudal interspaces, the triangularis sterni acts as an expiratory muscle of the rib cage. This muscle lies on the inner surface of the ventral rib cage. It extends from the dorsal part of the sternum to the costal cartilages of the third to seventh ribs. It is activated during all expiratory efforts.

The muscles of the abdominal wall consist of four layers: from outermost to innermost, the rectus abdominus, the external oblique, the internal oblique, and transversus abdominus. Of these, the transverse abdominus and the internal oblique have large expiratory mechanical advantages [40]. They exert an expiratory pressure on the abdominal wall and a caudal force on the lower ribs, thereby raising abdominal pressure and driving the dome of the diaphragm up into the thoracic cavity.

During normal breathing, only inspiratory muscles are activated during the inspiratory phase and only expiratory muscles during the expiratory phase. However, during phonation, and especially trained singing, both inspiratory and expiratory muscles are activated, presumably to increase the control of the pressure that drives the flow that drives vocal cord vibrations and the production of sound.

2.5 Compartmental Models

The total number of degrees of freedom of the chest wall is large [41], and the number of elastic parameters that would be required in order to construct a detailed quantitative model of the chest wall is very large. However, the distribution of activation of each group of respiratory muscles is fixed by the neurological controls, and thus the range of potential displacements is limited. Portions of the chest wall have been conceptually combined into compartments to obtain manageable models. These models provide an expression of our understanding of the mechanics of the chest wall and a vehicle for expressing quantitative relations between different observations.

In the one-compartment model, the chest wall is pictured as a structure with a configuration that is described by one degree of freedom, thoracic cavity volume. This model is depicted in the left panel of Fig. 2.11, in which the chest wall is a piston in a cylinder in series with a second piston that represents the lung, separated by the incompressible pleural space.

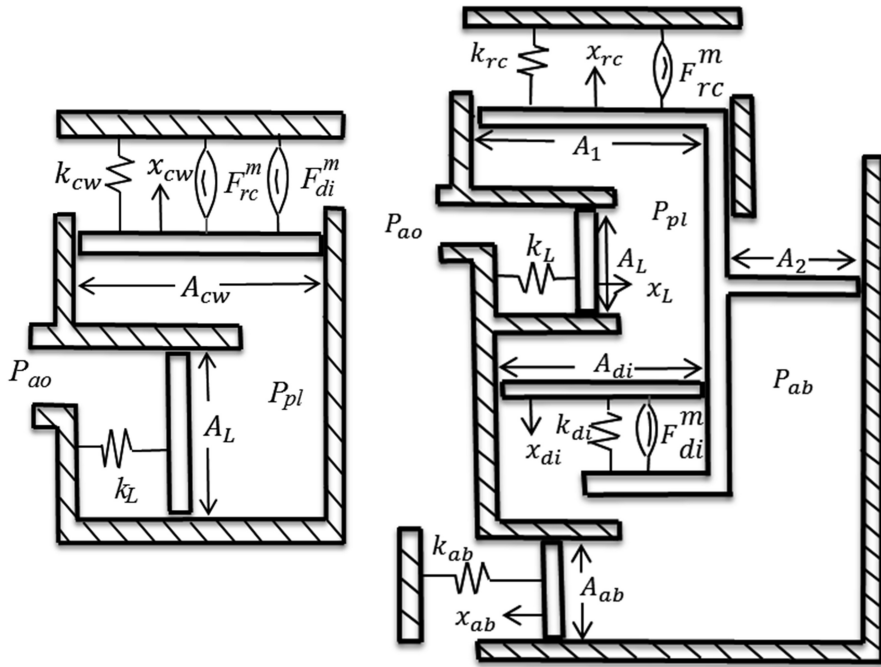


Fig. 2.11 Schematic diagram of the one-compartment model (*left panel*) and two-compartment model (*right panel*) of the chest wall. The hatched bars depict fixed walls, and the open bars depict pistons that represent the rib cage (*rc*), lung (*L*), diaphragm (*di*) and abdomen (*ab*). The pistons with area A_i are connected to the foundation with springs with spring constants k_i . The displacements of the pistons, x_i , are driven by active forces in the muscles of the rib cage (F_{rc}^m) and diaphragm (F_{di}^m) and by pressure applied at the airway opening (P_{ao}). All displacements and pressures are differences from positions and pressures at FRC

In the one-compartment model, for muscle activation with the airway closed, $P_{ao} = P_{pl} = -P^m$. From the comparison of this equation with Eq. (2.1), it follows that for this model, $P^m = -m \cdot \sigma \cdot \mu$ for both the muscles of the rib cage and the diaphragm.

In 1967, Konno and Mead [42] noted that one could inspire either by primarily expanding the rib cage or by primarily displacing volume with the abdominal wall, and at a fixed lung volume, one could shift volumes between these two. They measured the ventral displacements of a number of points on the ventral surface of the rib cage and abdomen for different breathing maneuvers. The relative displacements of points on the rib cage were nearly the same for all maneuvers; less so for the abdomen. By combining data for passive inflation and iso-volume maneuvers, they calibrated the displacements of one point on the rib cage and one on the abdomen so that the displacements of these points served as volume transducers. Since this work, the concept of the chest wall as a two-compartment system has been a cornerstone of the description of the mechanics of the chest wall.

A schematic diagram of the two-compartment model is shown in the right panel of Fig. 2.11. The insertional force exerted by the diaphragm on the rib cage is represented by the force acting on the shelf below the diaphragm. The appositional force is represented by abdominal pressure acting on area A_2 . The equilibrium equations for the four pistons in this model are the following.

$$P_{pl} + P_{rc}^m + \alpha \cdot P_{di} = E_{rc} \cdot V_{rc} \quad (2.3)$$

$$P_{di}^m - P_{di} = E_{di} \cdot (V_{ab} + \alpha \cdot V_{rc}) \quad (2.4)$$

$$P_{pl} + P_{di} = E_{ab} \cdot V_{ab} \quad (2.5)$$

$$P_{ao} - P_{pl} = E_L \cdot V_L \quad \text{where } V_L = V_{rc} + V_{ab} \quad (2.6)$$

The parameters in these equations are related to those shown in Fig. 2.11 by the following equations: $P_i^m = F_i^m/A_i$, $E_i = k_i/A_i^2$, $V_i = A_i \cdot x_i$, $A_{rc} = A_1 + A_2$, $\alpha = (A_{di} + A_2)/A_{rc}$, and P_{di} denotes transdiaphragmatic pressure, $P_{ab} - P_{pl}$. The volumes in the nether region are related by the equation, $V_{di} = V_{ab} + (A_2/A_{rc}) \cdot V_{rc}$.

Equation (2.3) is the same as the equation of equilibrium for the rib cage given by Loring and Mead [43]. In this equation, the parameter α describes the effective pressure exerted on the rib cage by the diaphragm as a fraction of P_{di} . Loring and Mead report the results of experiments intended to measure the value of α . In these experiments, V_{rc} , P_{pl} , and P_{ab} , were measured for passive inflation and during a maneuver in which the subjects inspired predominantly with their diaphragm. The average value of α at FRC was ≈ 0.6 . They note that subjects did not totally suppress intercostal activation during inspiration, and their value of α is presumably higher than the true value. Here, we take $A_2/A_{rc} = 0.3$, $A_{di}/A_{rc} = 0.2$, and $\alpha = 0.5$.

To represent the properties of a 24 kg dog with an inspiratory capacity of 1.2 L, the values of the elastances are taken as the following, all in cm H₂O/L.

$$E_{rc} = 10 \quad E_{di} = 8 \quad E_{ab} = 18$$

These values were chosen so that the predictions of the model for passive inflation of the chest wall match three observations: $V_{di} = 0.5 \cdot \Delta V_L$ [44], $P_{ab}/P_{pl} = 0.5$ [45], and $E_{cw} = 10$ cm H₂O/L. For a 72 kg human with an inspiratory capacity of 3.6 L, the values of the E 's are 1/3 those given for the dog.

Coordinated breathing with the intercostals and diaphragm is modeled by applying both P_{rc}^m and P_{di}^m with the airway open ($P_{ao} = 0$). Agostoni et al. [46] pointed out that the configuration of the chest wall during passive inflation is the configuration for which the elastic energy stored in the chest wall is minimum for a given chest wall volume. Therefore, the trajectory for passive inflation is the trajectory for which the work of chest wall expansion is minimum. It can be seen from Eqs. (2.3–2.6) that the chest wall is driven along the relaxation trajectory for $P_{rc}^m = (1 - \alpha) \cdot P_{di}^m = 0.5 \cdot P_{di}^m$. For these values of P^m and $E_L = 12$ cm H₂O/L, the model predicts $P_{ab}/P_{pl} = -0.4$, in agreement with observations [47].

For the case of muscle activation with the airway closed, the numerical solution to Eqs. (2.3–2.6), with the parameter values listed above, is the following.

$$P_{ao} = -0.73 \cdot P_{rc}^m - 0.63 \cdot P_{di}^m \quad (2.7)$$

Equation (2.7) has the form, $P_{ao} = -k_1 \cdot P_{rc}^m - k_2 \cdot P_{di}^m$. By comparison between this equation and Eq. (2.1), it can be seen that the muscle pressures in the two-compartment model are given by the following equations.

$$\begin{aligned} P_{rc}^m &= -(1/k_1) \cdot \sum_{rc} m \cdot \sigma \cdot \mu = -1.4 \cdot \sum_{rc} m \cdot \sigma \cdot \mu \\ P_{di}^m &= -(1/k_2) \cdot (m \cdot \sigma \cdot \mu)_{di} = -1.6 \cdot (m \cdot \sigma \cdot \mu)_{di}. \end{aligned}$$

The maximum potential value of $\sum_{rc} m \cdot \sigma \cdot \mu$ estimated above is $-24 \text{ cm H}_2\text{O}$. The corresponding value of P_{rc}^m is $34 \text{ cm H}_2\text{O}$. For coordinated muscle activation that produces no chest wall distortion ($P_{rc}^m = 0.5 \cdot P_{di}^m$), $P_{di}^m = 68 \text{ cm H}_2\text{O}$, and $(m \cdot \sigma \cdot \mu)_{di} = -42 \text{ cm H}_2\text{O}$. Thus, the maximum inspiratory pressure that can be generated with no chest wall distortion is $-66 \text{ cm H}_2\text{O}$, and the diaphragm contributes 64 % of P_{ao} , which matches the estimate of D'Angelo and Bellemare [48]. The value of P_{di}^m , $68 \text{ cm H}_2\text{O}$, is well below the estimate of the maximum value of P_{di} (Eq. 2.2).

The two-compartment model and Eq. (2.7) also provide a reconciliation of the two descriptions of diaphragm action obtained above. By Eq. (2.1), the maximum inspiratory potential of the diaphragm was estimated as $-70 \text{ cm H}_2\text{O}$. By Eq. (2.2), the maximum value of P_{di}^m was $110 \text{ cm H}_2\text{O}$. For $P_{ao} = -0.63P_{di}^m$, as given by Eq. (2.7), these two results are consistent.

The two-compartment model describes the contribution of the diaphragm to expansion of the rib cage and hence, explains the larger contribution of the diaphragm than the intercostals to chest wall expansion. It also describes the contribution of the volume displaced by the zone of apposition to the volume balance for the abdomen. In the model, 45 % of the volume displaced by the diaphragm is taken by the expansion of the lower rib cage in the zone of apposition, in agreement with the fraction measured by Knight et al. in dogs [49] and the estimates of Mead and Loring for humans [50]. The model also depicts the fact that the diaphragm inserts on an elastic foundation and that the displacement of the foundation, as well as the displacement of the dome of the diaphragm, determine diaphragm muscle shortening. In the model, the displacement of the lower rib cage contributes 20 % of diaphragm shortening, in agreement with the value inferred from data on the displacements of the diaphragm dome and the lower ribs [17].

For coordinated breathing, the two-compartment model provides an accurate description of chest wall kinematics. For more extreme maneuvers, this model is inadequate. In subjects with tetraplegia [34, 35] and in dogs breathing with the diaphragm alone [33], the upper ribs move caudally and inward during inspiration whereas the lower ribs move cranially and outward. For these maneuvers, the chest

wall has been modeled by a three-compartment model in which the rib cage is subdivided into upper and lower compartments [51, 52].

One of the forces exerted on the lower rib cage is the appositional force, and this force is proportional to the area of apposition. With increasing lung volume, the area of the zone of apposition decreases, the force exerted by the diaphragm on the lower rib cage decreases, and the lower rib cage moves inward during diaphragm activation [36]. This decrease in the effect of the diaphragm also is manifested in Hoover's sign, an inward displacement of the lower rib cage during inspiration that is seen in some patients with COPD.

These models describe the actions of the inspiratory muscles. The data that would be required to formulate comparative models for the action of the expiratory muscles have not been obtained.

2.6 Work of Breathing

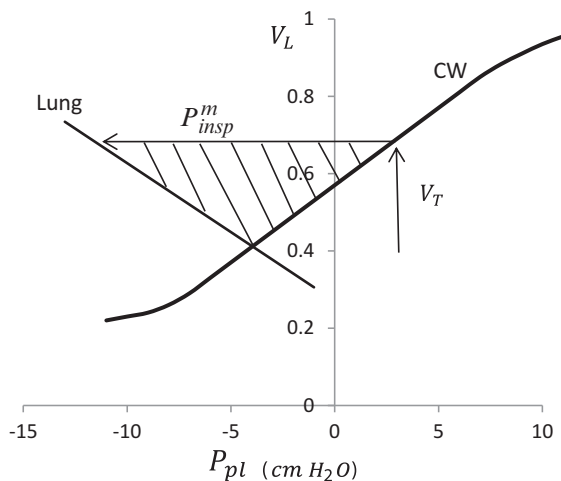
The rate of work (\dot{W}) of the respiratory muscles for quiet breathing with breathing frequency f , tidal volume V_T , and end-expiratory volume equal to FRC is given by Eq. (2.8).

$$\dot{W} = \frac{1}{2} \cdot f \cdot E_{rs} \cdot V_T^2 \quad E_{rs} = E_L + E_{cw} \quad (2.8)$$

The work per breath is usually depicted by the Campbell diagram shown in Fig. 2.12.

The work per breath is the shaded area in the diagram. For quiet breathing, an additional 25 % can be added to the shaded area to account for work done against the resistive load. Also, during active inspiration, chest wall distortion from the passive configuration at a scale smaller than the compartmental scale adds another 25 % to the work done by the muscles [53]. Because the work per breath is proportional to the square of the difference between end-inspiratory volume and FRC (or end-expiratory volume and FRC), the work for a given tidal volume would be minimized if half the tidal volume were taken below FRC and half above. Dogs [4] and horses use their expiratory muscles during quiet breathing and end-expiratory volume is below FRC. Humans use only the inspiratory muscles during quiet breathing, but with the onset of exercise, the expiratory muscles are recruited and end-expiratory volume is lower than FRC. The diagram also shows the added work required if end-expiratory volume is above FRC, as occurs because of dynamic hyperinflation in COPD patients. For quiet breathing, the work of breathing is quite small, $\sim 2 \cdot 10^{-2}$ W. During exercise, this can increase by a factor of 25, but in normals, the work of breathing is always a small part of total metabolism.

Fig. 2.12 Campbell diagram with the work done per breath shown by the shaded area



2.7 Mechanics of the Pleural Space

The pleural space is a thin layer of fluid that lies between the lung and the chest wall. In breathing, the ribs move cranially and the lung is stretched caudally. Thus, the lungs slide along the inner surface of the rib cage. The liquid in the pleural space lubricates this sliding. The pleural space is thin, $\sim 15 \mu$ in the dog, except along lines where a lobar fissure meets the pleural surface where a broader channel runs along the fissure. The pressure distribution in the pleural space is dictated by the mechanics of the lung and chest wall. As described in the first chapter, the pressure gradient must balance the gravitational force on the lung, $\rho_L g$. The magnitude of this pressure gradient at FRC is therefore about $0.25 \text{ cm H}_2\text{O}/\text{cm}$. This pressure gradient is too small to balance the gravitational body force ρg that acts on the fluid with the density of water in the pleural space, and the fluid drains downward. However, a pumping action driven by the sliding between the lung and the rib cage pumps fluid out from the channels along the lobar fissures into the thin layer on the surface of the lung [54, 55]. Fluid drains downward along the surface and flows back up along the fissure to complete the circulatory flow that maintains the pleural space. The volume of pleural fluid is controlled by absorption and emission of fluid across the parietal pleura.

Appendix

Values of the parameters of the arcs that describe the center lines of the ribs of dogs (Tables 2.1 and 2.2) and humans (Tables 2.3 and 2.4).

Table 2.1 Values of the parameters for a 12 kg dog at FRC

Rib #	A (cm)	ξ_o (cm)	R_1 (cm)	R_2 (cm)	α	β
3	17.5	-0.2	4.7	3.6	7.9	-12.1
4	16.5	0.2	5.3	4.5	2.0	-18.5
5	14.6	0.2	5.8	5.2	-1.7	-20.5
6	13.2	0.2	6.2	5.8	-5.1	-24.5
7	11.5	0.0	6.5	6.3	-8.0	-24.4
8	9.3	-0.1	6.8	6.5	-9.5	-23.4

Table 2.2 Difference between parameter values at TLC and FRC

Rib #	δA	$\delta \xi_o$	$\delta \alpha$	$\delta \beta$
3	-0.1	0.1	3.8	16.3
4	0.0	0.0	6.4	14.7
5	0.1	0.1	6.0	13.3
6	0.2	0.0	6.1	12.1
7	0.3	0.1	6.4	9.4
8	0.6	0.0	5.5	5.5

Table 2.3 Parameter values for human ribs at FRC

Rib #	A (cm)	ξ_o (cm)	R_1 (cm)	R_2 (cm)	α	β
2	37.8	3.6	7.2	10.6	-40.3	-23.1
3	34.4	3.1	9.2	11.6	-37.8	-21.2
4	30.5	2.5	11.7	12.7	-40.3	-16.3
5	25.9	1.5	12.8	12.6	-41.9	-9.4
6	20.3	-0.4	14.0	12.8	-44.6	-0.3
7	14.4	-2.2	14.7	13.0	-46.1	8.8
8	9.8	-2.6	15.8	13.3	-50.7	10.8
9	6.6	-3.6	14.4	13.4	-50.7	10.3

Table 2.4 Differences between values at TLC and FRC for human ribs

Rib #	δA	$\delta \xi_o$	$\delta \alpha$	$\delta \beta$
2	-1.0	-0.4	14.3	13.7
3	-0.1	-0.4	11.4	13.3
4	0.5	0.4	10.7	10.1
5	1.0	0.7	9.6	8.9
6	1.4	1.6	9.4	6.9
7	1.5	1.5	7.9	6.6
8	1.7	2.1	7.9	6.2
9	1.5	1.5	6.0	6.3

References

1. Cappello M, De Troyer A. On the respiratory function of the ribs. *J Appl Physiol.* 2002;92:1642–6.
2. Margulies SS, Rodarte JR, Hoffman EA. Geometry and kinematics of dog ribs. *J Appl Physiol.* 1989;67:707–12.
3. Wilson TA, Legrand A, Gevenois P-A, De Troyer A. Respiratory effects of the external and inter intercostal muscles in humans. *J Physiol.* 2001;530:319–30.
4. De Troyer A, Ninane V. Triangularis sterni: a primary muscle of breathing in the dog. *J Appl Physiol.* 1986;60:14–21.
5. Wilson TA, De Troyer A. Effect of respiratory muscle tension on lung volume. *J Appl Physiol.* 1992;73:2283–8.
6. De Troyer A, Legrand A. mechanical advantage of the canine triangularis sterni. *J Appl Physiol.* 1998;84:562–8.
7. De Troyer A, Legrand A, Wilson TA. Rostrocaudal gradient of mechanical advantage in the parasternal intercostal muscles of the dog. *J Physiol.* 1999;495:239–89.
8. De Troyer A, Legrand A, Wilson TA. Respiratory mechanical advantage of the canine external and internal intercostal muscles. *J Physiol.* 1999;518:283–9.
9. De Troyer A, Legrand A, Gevenois PA, Wilson TA. Mechanical advantage of the human parasternal intercostal and triangularis sterni muscles. *J Physiol.* 1998;513:915–25.
10. De Troyer A, Gorman RB, Gandevia SC. Distribution of inspiratory drive to the external intercostal muscles in humans. *J Physiol.* 2003;546:943–54.
11. De Troyer A, Legrand A. Inhomogeneous activation of the parasternal intercostals during breathing. *J Appl Physiol.* 1995;79:55–62.
12. Johnson Jr RL, Hsia CCW, Takeda SI, Wait JL, Glenn RW. Efficient design of the diaphragm: distribution of blood flow relative to mechanical advantage. *J Appl Physiol.* 2002;93:925–30.
13. DiMarco AF, Romaniuk JR, Supinski GS. Mechanical action of the interosseus intercostal muscles as a function of lung volume. *Am Rev Respir Dis.* 1990;142:1041–6.
14. DiMarco AF, Supinski GS, Budzinska K. Inspiratory muscle interaction in the generation of changes in airway pressure. *J Appl Physiol.* 1989;66:2573–8.
15. Hamberger GE. *De Respirationis Mechanismo et usu* Gennino, Christoph Croeker, 1740
16. De Troyer A, Leduc D. Effects of inflation on the coupling between the ribs and the lung in dogs. *J Physiol.* 2004;555:481–8.
17. De Troyer A, Wilson TA. Coupling between the ribs and the lung in dogs. *J Physiol.* 2002;540:231–6.
18. Wilson TA, De Troyer A. The two mechanisms of intercostal muscle action on the lung. *J Appl Physiol.* 2004;96:483–8.
19. De Troyer A, Leduc D, Cappello M, Minne B, Rooze M, Gevenois PA, Wilson TA. Mechanisms of the inspiratory action of the diaphragm during isolated contraction. *J Appl Physiol.* 2009;107:1736–42.
20. Boriek AM, Rodarte JR, Margulies SS. Zone of apposition in the passive diaphragm in the dog. *J Appl Physiol.* 1996;81:1929–40.
21. Gauthier AP, Verbanck S, Estenne M, Segebarth C, Macklem PT, Paiva M. Three dimensional reconstruction of the in vivo human diaphragm shape at different lung volumes. *J Appl Physiol.* 1994;76:495–506.
22. Mead J. Functional significance of the area of apposition of diaphragm to rib cage. *Am Rev Respir Dis.* 1979;119S:31–2.
23. Wilson TA, Boriek A, Rodarte JR. Mechanical advantage of the canine diaphragm. *J Appl Physiol.* 1998;85:2284–90.
24. Leiter JC, Jacopo PM, Tenney SM. A comparative analysis of contractile characteristics of the diaphragm and of respiratory system mechanics. *Respir Physiol.* 1986;64:267–76.

25. Hershenson MB, Kikuchi Y, Loring SH. Relative strengths of the chest wall muscles. *J Appl Physiol.* 1988;65:852–62.
26. Boriek AM, Wilson TA, Rodarte JR. Displacements and strains in the costal diaphragm of the dog. *J Appl Physiol.* 1994;76:223–9.
27. Boriek AM, Kelly NG, Rodarte JR, Wilson TA. Biaxial constitutive relations for the passive canine diaphragm. *J Appl Physiol.* 2000;89:2187–90.
28. Angelillo M, Boriek AM, Rodarte JR, Wilson TA. Theory of diaphragm structure and shape. *J Appl Physiol.* 1997;83:1486–91.
29. Wait JL, Saworn D, Poole DC. Diaphragm thickness heterogeneity at functional residual capacity and total lung capacity. *J Appl Physiol.* 1995;78:1030–6.
30. Boriek AM, Liu S, Rodarte JR. Costal diaphragm curvature in the dog. *J Appl Physiol.* 1993;75:527–33.
31. Road J, Newman S, Derenne JP, Grassino A. In vivo length-force relationship of canine diaphragm. *J Appl Physiol.* 1985;58:1646–53.
32. Boriek AM, Black B, Hubmayr R, Wilson TA. Length and curvature of the dog diaphragm. *J Appl Physiol.* 2006;101:794–8.
33. De Troyer A. The action of the canine diaphragm on the lower ribs depends on activation. *J Appl Physiol.* 2011;111:1266–71.
34. Estenne M, De Troyer A. Relationship between respiratory muscle electromyogram and rib cage motion in tetraplegia. *Am Rev Respir Dis.* 1985;132:53–9.
35. Mortola JP, Sant' Ambrogio G. Motion of the rib cage and the abdomen in tetraplegic patients. *Clin Sci Mol Med.* 1978;54:25–32.
36. De Troyer A, Wilson TA. Action of the isolated canine diaphragm on the lower ribs at high lung volumes. *J Appl Physiol.* 2014;592:4481–91.
37. De Troyer A, Wilson TA. Effect of acute inflation on the mechanics of the inspiratory muscles. *J Appl Physiol.* 2009;107:315–23.
38. Legrand A, Ninane V, De Troyer A. Mechanical advantage of sternomastoid and scalene muscles in dogs. *J Appl Physiol.* 1997;82:1517–22.
39. Legrand A, Schneider E, Gevenois PA, De Troyer A. Respiratory effects of the scalene and sternomastoid muscles in humans. *J Appl Physiol.* 2003;94:1467–72.
40. Leevers AM, Road JD. Mechanical response to hyperinflation of the two abdominal muscle layers. *J Appl Physiol.* 1989;66:2189–95.
41. De Troyer A, Wilson TA. The parasternal and external intercostal muscles drive the ribs differently. *J Appl Physiol.* 2000;523:799–806.
42. Konno K, Mead J. Measurement of the separate volume changes of the rib cage and abdomen during breathing. *J Appl Physiol.* 1967;22:407–22.
43. Loring SH, Mead J. Action of the diaphragm on the rib cage inferred from a force-balance analysis. *J Appl Physiol.* 1982;53:756–60.
44. Warner DO, Krayner S, Rehder K, Ritman R. Chest wall motion during spontaneous breathing and mechanical ventilation in dogs. *J Appl Physiol.* 1989;66:1179–89.
45. Wilson TA, De Troyer A. Effects of insertional and appositional forces of the canine diaphragm on the lower ribs. *J Physiol.* 2013;591:3539–48.
46. Agostoni E, Mognoni P, Torri G, Agostoni A. Static features of the passive rib cage and diaphragm-abdomen. *J Appl Physiol.* 1965;20:1187–93.
47. Jiang TX, Demedts M, DeCramer M. Mechanical coupling of upper and lower canine rib cages and its functional significance. *J Appl Physiol.* 1988;64:620–6.
48. D'Angelo E, Bellemare F. Electrical and mechanical output of the inspiratory muscles in anesthetized dogs. *Respir Physiol.* 1990;79:177–94.
49. Knight H, Petroll WM, Rochester D. Relationships between abdominal and diaphragmatic volume displacements. *J Appl Physiol.* 1991;71:565–72.
50. Mead J, Loring SH. Analysis of volume displacement and length changes of the diaphragm during breathing. *J Appl Physiol.* 1982;53:750–5.

51. Ward ME, Ward JW, Macklem PT. Analysis of human chest wall motion using a two-compartment rib cage model. *J Appl Physiol.* 1992;72:1338–47.
52. Wilson TA. Compartmental models of the chest wall and the origin of Hoover's sign. *Respir Physiol Neurobiol.* 2015;210:23–9.
53. Wilson TA, Angelillo M, Legrand A, De Troyer A. Muscle kinematics for minimum work of breathing. *J Appl Physiol.* 1999;87:554–60.
54. Butler JP, Huang J, Loring SH, Lai-Fook SJ, Wang PM, Wilson TA. Model for a pump that drives circulation of pleural fluid. *J Appl Physiol.* 1995;78:23–9.
55. Wang PM, Lai-Fook SJ. Upward flow of pleural liquid near lobar margins due to cardiogenic motion. *J Appl Physiol.* 1992;73:2314–9.

Respiratory Mechanics

Wilson, T.A.

2016, VIII, 64 p. 29 illus., 13 illus. in color., Softcover

ISBN: 978-3-319-30507-3